Journal of Inorganic Biochemistry 249 (2023) 112366

Contents lists available at ScienceDirect

Journal of Inorganic Biochemistry

journal homepage: www.elsevier.com/locate/jinorgbio

Aqueous chemistry of nalidixic acid and its complexes with biological relevant cations: A combination of potentiometric, UV spectrophotometric, MS and MS/MS study

Federica Carnamucio [a,1], Donatella Aiello [b,1], Claudia Foti [a], Anna Napoli [b,*], Ottavia Giuffrè [a,*]

[a] Dipartimento di Scienze Chimiche, Biologiche, Farmaceutiche ed Ambientali, Università di Messina, Viale F. Stagno d'Alcontres 31, 98166 Messina, Italy
[b] Dipartimento di Chimica e Tecnologie Chimiche, Università della Calabria, Via P. Bucci, 87036 Arcavacata di Rende, CS, Italy

ARTICLE INFO

Keywords:
Nalidixic acid
Speciation
Sequestration
Potentiometry
UV-Vis spectroscopy
MS, MS/MS spectrometry

ABSTRACT

Nalidixic acid (**NAL**) is a broad-spectrum antimicrobial widely used for urinary tract infections. As demonstrated, complexation of **NAL** with Zn^{2+}, Mn^{2+} and Cu^{2+} was often used to get new formulations with an enhanced efficiency and potency. Therefore, the elucidation of behavior of **NAL** in solution and of its interaction with metal cations are crucial to better understand the influence of complexation on **NAL** efficiency and to find the optimal conditions to propose novel formulations. As a preliminary study, spectrophotometric titrations were carried out on **NAL** to determine the values of the protonation constants and to define its acid-base behavior. Then, the interaction with the three metal cations Zn^{2+}, Mn^{2+} and Cu^{2+} was investigated by potentiometric and spectrophotometric titrations, varying the conditions of temperature, ionic strength and metal-ligand ratio, thus allowing to get the most robust speciation model and to determine the formation constants with Zn^{2+}, Mn^{2+}, and Cu^{2+} under different conditions, the sequestering ability of **NAL** towards metal cations, the formation enthalpic and entropic changes. A simulation under serum conditions was reported to show the relevance of the investigated species. Finally, LD-MS (laser desorption ionization mass spectrometry) and MS/MS analyses highlighted for all systems the formation of the complex species between Zn^{2+}, Mn^{2+} and Cu^{2+} with **NAL**. MS/MS investigations assigned the sites of coordination of the ligand with the metal cation. More precisely, deprotonated **NAL** coordinates the metal cation via the oxygens of the carboxylate and the carbonyl groups.

1. Introduction

Among the various antibacterial agents, quinolones have played a crucial role in the battle against infectious diseases due to their high efficacy. Nalidixic acid (**NAL**) or 1-Ethyl-7-methyl-4-oxo-[1,8]naphthyridine-3-carboxylic acid, represented in Fig. 1, is the first broad-spectrum quinolone synthesized for the treatment of urinary tract infectious [1,2]. Over the years, the intensive use of **NAL** as well as other antibiotics, has allowed many microorganisms to develop high resistance capacities which has led to a significant decrease in effectiveness [3–8]. This is the main reason why infectious diseases are still the leading cause of death in the world. In recent years, research has therefore focused on the development of new formulations capable of improving the effect and solving the problem related on drug resistance [3,5,9–12]. In this perspective, metal-organic frameworks (MOFs) have found application on antibiotic administration. MOFs have allowed not only to increase solubility in water and bioavailability after oral administration, but the complexation with metal cations, such as Mn^{2+}, Zn^{2+}, Cu^{2+},Fe^{2+} has led to a significant enhancement in antimicrobial activity [3,4,8,13–17]. The complex species with Cu^{2+} have also aroused considerable interest [5,18–23], due to its high affinity towards DNA and RNA, representing an important chemotype capable of inducing apoptotic processes in tumor cells. In particular, the high toxicity of Cu^{2+} species is closely related to its ability to produce reactive oxygen species (ROS) and to directly cleave DNA and RNA strands [11,19,24–26]. The use of Cu^{2+} complexes as anticancer agents has made it possible to avoid all those unwanted side effects generally induced by non-selective drugs, like cisplatin [4,19,27,28]. In fact, it was established that $Cu^{2+}$are less toxic to healthy cells than cancer ones. In addition, the possibility of synthesizing Cu-based ternary complexes of nalidixic acid with O or N donor

* Corresponding authors.
E-mail addresses: amc.napoli@unical.it (A. Napoli), ogiuffre@unime.it (O. Giuffrè).
[1] F.C. and D.A. contributed equally.

https://doi.org/10.1016/j.jinorgbio.2023.112366
Received 16 June 2023; Received in revised form 22 August 2023; Accepted 5 September 2023
Available online 6 September 2023
0162-0134/© 2023 The Authors. Published by Elsevier Inc. This is an open access article under the CC BY license (http://creativecommons.org/licenses/by/4.0/).

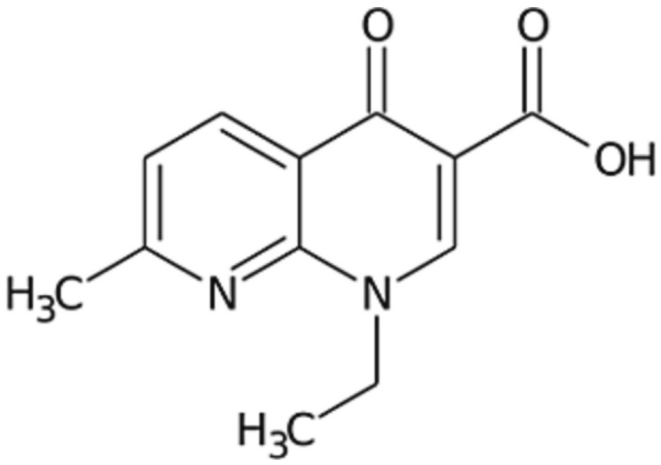

Fig. 1. 1-Ethyl-7-methyl-4-oxo-[1,8]naphthyridine-3-carboxylic acid (**NAL**).

ligands or co-ligands has allowed to a significant improvement of the cytotoxicity [9,18,29–32]. Furthermore, drug-metal complexes were often exploited in nanomedicine. It is now known how formulations of chemotherapeutics by drug delivery systems can improve the pharmacokinetic profile and achieve controlled release. In spite, in the literature, various liposomal formulations based on nalidixic acid have been proposed, they are characterized by low entrapment efficiency values [33]. The development of more effective **NAL** formulation is needed. The interaction between Mn^{2+} and chemotherapeutic agents, e.g. doxorubicin, has proven to be a great strategy for improving formulation and thus obtain more performing results [34]. Chiu et al. [35] hypothesized that the interaction between the drug and Mn^{2+} represents the driving force for the drug loading, allowing to achieve a higher entrapment efficiency. The aim of this investigation was to carry out a thermodynamic study useful as preliminary research for the proposal of new NAL-based liposomal formulations. A preliminary speciation study, aimed at defining the species that **NAL** forms in solution with Zn^{2+}, Cu^{2+} and Mn^{2+} was conducted to determine the extent of the interaction between **NAL** and the metal cations and the percentages of formation of the complexes, as a function of parameters such as pH, temperature and metal/drug ratio. This allows to identify the optimal conditions to propose new nanoformulations that may find use in the treatment of various cancers. As well known, Mn^{2+}, Zn^{2+}, and Cu^{2+} are essential in the body in carrying out various functions [24]. As an example, they make it possible to facilitate redox reactions, transfer of chemical groups and stabilize the protein structures. Mn^{2+} is an essential micronutrient, capable of reducing the reactive oxygen species in Mn superoxide dismutase (MnSOD), in the catalysis dependent on electron transfer (for example in ribonucleotide reductase I) and in the oxidation of water by Photosystem II [36]. Zn^{2+} is a trace element, involved in various enzymatic actions, necessary for various physiological functions, including protection of sulfhydryl groups from oxidation and inhibition of oxidative processes that lead to the formation of reactive oxygen [29]. Copper is a trace metal, essential to several vital biological processes. Present in the oxidation state of Cu^{+} and Cu^{2+}, it is often used as a catalytic cofactor in numerous biological processes both in bacteria and in humans [22].

Literature data include the study of gas-phase metal ion chemistry and the formation of metal ion adducts to assist in the detection and structural elucidation of organic compounds [37]. Mass Spectrometry (MS) experiments are able to clarify the stoichiometry of a specific complex, while tandem mass spectrometry (MS/MS) provide information on the coordination sites [38–40]. Structural information on metal-**NAL** compounds is difficult, even under the softest ionization conditions, because complexes are susceptible to fragmentation during the ionization process. Therefore, the molecular adducts may be missing completely, or their relative abundances may be very low in the full-scan mass spectra. Furthermore, the ligand (**NAL**) exhibits a highly conjugated double bonds structure offering the possibility to employ itself as an effective matrix in experiment producing ions after sample laser ablation. Although ESI (electrospray ionization) and MALDI (matrix assisted laser desorption ionization) mass spectrometry are generally used [41–43], here LD TOF/TOF (Laser Desorption Ionization Time of Flight- Time of Flight) technique was chosen for its accuracy and sensitivity, no-time consuming sample preparation and data acquisition, and in relation to the **NAL** structure. Thus, LD MS can be exploited to determine either the composition and structure elucidation of Mn^{2+}-**NAL**, Zn^{2+}-**NAL**, and Cu^{2+}-**NAL** complexes. Thermodynamic parameters (i.e., log$K$, ΔG,ΔH, $T\Delta S$, and also the dependence of formation constants on temperature and ionic strength) of Mn^{2+}, Zn^{2+}, and Cu^{2+} with **NAL** and the possible structures of the complexes will be discussed based on potentiometric, UV spectrophotometric and mass spectrometric results.

2. Materials and methods

2.1. Chemicals

Nalidixic acid sodium salt (**NAL**) and metal cation solutions were prepared by weighting and dissolving the commercial products, Nalidixic acid sodium salt (purity ≥99%, Sigma-Aldrich®), Manganese(II) chloride tetrahydrate (purity ≥99%, Sigma-Aldrich®), Zinc(II) chloride monohydrate (puriss, Merk), Copper(II) sulfate pentahydrate (puriss. P. a. cryst. >99%, Fluka®), respectively. Metal cation solutions were standardized by EDTA titrations. NaOH and HCl solutions, used for potentiometric and spectrophotometric titrations, were prepared by dilution from the Fluka® concentrated vials and standardized with potassium acid phthalate and sodium carbonate, respectively, pre-dried in an oven for at least one hour at 110 °C. The NaCl solutions were prepared by direct weighing of Sigma-Aldrich® product (purity ≥99.5%), first dried in an oven at 110 °C. Distilled water (conductivity <0.1 μS cm^{-1}) and class A glassware were used for all solutions.

2.2. Potentiometric apparatus

All the potentiometric titrations were performed by Metrohm-Titrando 809 with a Thermo-Fisher combined glass electrode and a MetrohmDosino 800 automatic dispenser. Thermostated cells, by thermostat model D1-G Haake with a capacity of 25 mL, were used for all titrations. During the measurements pure N_2 was bubbled to avoid CO_2 and O_2 in solution. The data were acquired by using Metrohm TIAMO 2.0 software, controlling parameters such us e.m.f. stability, titrant delivery, and data acquisition, with an estimated accuracy of ±0.15 mV and ±0.002 mL. 25 mL solutions containing **NAL**, HCl and NaCl as supporting electrolyte at $t = 15, 25, 37$ °C and $0.15 \leq I/\text{mol L}^{-1} \leq 0.99$ were titrated for the preliminary acid-base study. Then, various potentiometric titrations are performed on 25 mL of NaCl solutions containing metal cation (M)-**NAL** in different ratios, at $t = 15, 25, 37$ °C and ionic strength in the interval $0.15 \leq I/\text{mol L}^{-1} \leq 0.99$. The experimental conditions of potentiometric titrations are summarized in Table 1. The effective ionic strength values of experimental measurements were reported in Table 2. For each system, at least four measurements were performed in different conditions of metal-ligand ratio. All titrations were carried out using NaOH solution as titrant. For each measurement a calibration was associated by titration with 0.1 mol L^{-1} NaOH on solutions containing 0.01 mol L^{-1} HCl, NaCl and H_2O in the same conditions of ionic strength, in order to calculate the standard electrode potential (E^0) and the pK_w values used in the input file of the corresponding measurements.

2.3. UV-Vis apparatus

A Varian Cary 50 UV–Vis spectrophotometer equipped with an

Table 1
Experimental conditions for potentiometric and spectrophotometric titrations.

Technique	t / °C	I / mol L^{-1}	C_M / mmol L^{-1}	C_L / mmol L^{-1}	M/L ratio	pH range
Potentiometry	15,25,37,45	0.15–0.99	0.5–1	0.5–1	0.75–1.5	3–10
Spectrophotometry	15,25,37,45	0.15	–	0.03–0.05	–	3–10
	25	0.15	0.02–0.03	0.03–0.05	0.33–1	3–10

Table 2
Experimental protonation constants of **NAL** (L) obtained by spectrophotometric titrations and experimental formation constants of Zn^{2+}-L, Mn^{2+}-L, and Cu^{2+}-L species obtained by potentiometric titrations.

Reaction[1]	t /°C	I / mol L^{-1}	logβ
	15	0.15	6.025(2)[2]
	25	0.16	5.946(7)
L + H = LH	25	0.50	5.809(4)
	25	0.99	5.705(4)
	37	0.15	5.82(2)
	45	0.15	5.83(10)
Zn + L = ZnL	15	0.16	3.30(2)
	25	0.16	3.45(4)
	25	0.49	2.86(4)
	25	0.98	3.53(3)
	37	0.16	2.91(5)
Zn + L + H_2O = ZnLOH + H	15	0.16	−5.59(4)
	25	0.16	−5.21(6)
	25	0.49	−5.49(2)
	25	0.98	−5.02(4)
	37	0.16	−5.31(4)
Mn + L = MnL	15	0.16	4.40(4)
	25	0.16	4.24(2)
	25	0.49	4.59(3)
	25	0.99	4.60(2)
	37	0.16	4.00(5)
Cu + L = CuL	15	0.16	5.49(2)
	25	0.16	5.16(10)
	25	0.50	5.44(2)
	25	0.98	5.41(3)
	37	0.16	5.32(4)
	45	0.15	5.13(18)
Cu + 2 L = CuL_2	15	0.16	10.27(3)
	25	0.16	10.24(7)
	25	0.50	9.67(2)
	25	0.98	9.34(7)
	37	0.16	11.06(4)
	45	0.15	11.47(7)

[1] Charges omitted for simplicity;[2] ≥ 95% of confidence interval.

optical fiber with a fixed 1 cm path length was used for spectrophotometric titration. The instrument was interfaced to a PC by the Varian Cary WinUV software. The use of a Methrom glass electrode and a Metrohm-Titrando 809 potentiometer allows to record simultaneously the couple data of absorbance (Abs) and pH vs. volume of titrant (mL), for each titration point. All analyses were carried out in a thermostated cell in which N_2 was bubbled in solution to avoid CO_2 and O_2. The experimental conditions of the titrations are reported in Table 1. For each system, at least four measurements were performed in different conditions of metal-ligand ratio. Protonation constant values were determined at 15, 25, 37 and 45 °C.The spectra were obtained by scanning from 225 to 400 nm and a baseline containing only HCl, NaCl and H_2O in the same conditions of ionic strength was recorded before each measurement to consider the contribution of the matrix.

2.4. Calculations

BSTAC and STACO programs were used to calculate protonation and formation constant values of **NAL**, M-**NAL** and the titration parameters (analytical concentration of the reagents, standard potential E^0, junction potential). LIANA program has provided the parameters characterizing the dependence of the protonation and formation constant values on the temperature and ionic strength [44]. HypSpec program [45] was used for UV data, enabling to refine protonation and formation constants as well as the molar absorption coefficient values (ε) of all species. In order to get the speciation diagrams Hyss program was used [46].

2.5. Mass spectrometry apparatus

The metal–Nalidixic acid complexes ([LH, Zn^{2+}]; [LH, Mn^{2+}]; [LH, Cu^{2+}]) were prepared starting from 1 mmol of metal chloride dissolved in water, while a solution of 2 equivalents ligand was added over stirring. Complexes were not isolated and 1 μL of the resulting reaction mixture was directly loaded on probe and analyzed by positive-ion mode mass spectrometry. LD-MS (laser desorption ionization mass spectrometry) analyses were performed using a 5800 MALDI TOF–TOF Analyzer (AB SCIEX) equipped with a neodymium–yttrium–aluminum–garnet laser (laser wavelength 349 nm). At least 4000 laser shots were typically accumulated with a laser pulse rate of 400 Hz in the MS mode with a mass accuracy of 5 ppm. CID (collision induced dissociation) MS/MS experiments were performed at a collision energy of 1 kV, using ambient air as collision gas. Spectra were acquired accumulating up to 5000 laser shots and after acquisition, all spectra were handled using Data Explorer version 4.0. All spectra were recorded in positive mode. The free ligand was also analyzed by LD-MS experiment, in order to evaluate ionization behavior. 10 mg of Nalidixic acid sodium salt powder was solubilized in 1 mL of water and then added with 30 μL of HCl ($1{\cdot}10^{-3}$ mol L^{-1}) under stirring drop by drop and with 30 μL of NH_4OH ($1{\cdot}10^{-3}$ mol L^{-1}). Sodium ions are removed by solution stirring overnight and then the solution was directly analyzed by LD mass spectrometry.

3. Results and discussion

3.1. Acid-base behavior of NAL and speciation of Mn^{2+}-, Zn^{2+}- and Cu^{2+}-NAL systems

A preliminary acid-base study on **NAL** was performed to assess the thermodynamic behavior by determining the protonation constant values, needful for metal-ligand investigation. As reported in the review on quinolones by Turel, **NAL** was characterized by one protonation constant in the range of pH = 2–9. Under strongly acid pH values **NAL** is protonated to give a naphthyridinium cation having a $pK_a = -0.86$ [47]. For this reason, the only experimentally determinable protonation constant is that which refers to the carboxylate group.

The equilibrium reaction, associated with the protonation constant value, is the following, where **NAL** is indicated as L:

$$L^- + H^+ = LH \qquad \beta^{LH} \tag{1}$$

The experimental protonation constant values, listed in Table 2, are obtained by spectrophotometric titrations at different temperature (15, 25, 37 and 45 °C) and ionic strength ($0.15 \leq I/\text{mol } L^{-1} \leq 0.99$) conditions.

Spectrophotometric titrations, performed on solutions with different concentrations of ligand, allowed to calculate the protonation constant value as well as to assess the spectral behavior of L and LH species. Spectrophotometry was preferred to potentiometry due the possibility to use significantly lower concentrations of **NAL**, characterized by poor solubility in aqueous solution at acid pH values and thus obviate the problem of precipitation. In Fig. 2b, by way of example, some of spectra obtained at selected pH in the spectral range $225 \leq \lambda \leq 400$ nm, are

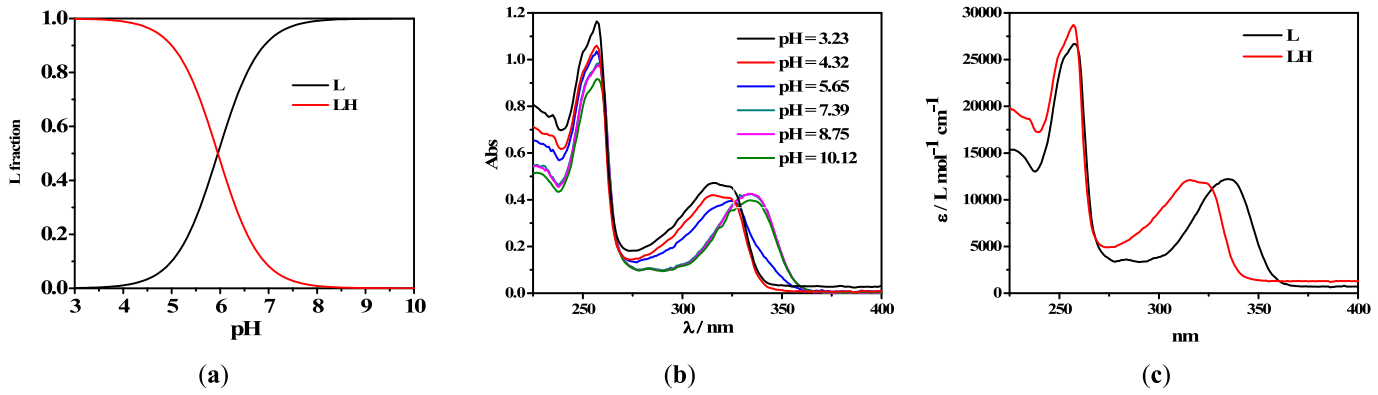

Fig. 2. **NAL** (L): (a) Distribution diagram; (b) UV spectra at selected pH values at C = 0.03 mmol L^{-1}; (c) ε vs. λ. Experimental conditions: t = 37 °C, I = 0.15 mol L^{-1} in NaCl.

reported. Two maxima of absorption are visible at around 250 and 320 nm, characterized by hypochromic and bathochromic effects as a consequent of pH increase.

One isosbestic point, representing L/LH equilibria, is also distinguishable. The molar absorbances of the protonated and unprotonated species of the ligand were reported in Fig. 2c. In detail, at λ = 256 nm, for L and LH species an absorption maximum of 26,300 and 28,300 L mol^{-1} cm^{-1}, respectively, was observed. L deprotonated species reaches a second maximum corresponding to 12,000 L mol^{-1} cm^{-1} at λ = 330 nm, while LH reaches 12,100 L mol^{-1} cm^{-1} at λ = 315 nm.

Once the acid-base properties of the ligand as well as the hydrolytic behavior of the metal cations (hydrolytic constants reported in Tables S1-S3 in Supplementary Material) are known, it was possible to study the interaction between **NAL** and metal cations. In the study of the complexes of **NAL** with Mn^{2+}, Zn^{2+} and Cu^{2+} it was possible to use even higher ligand concentrations than those used for protonation

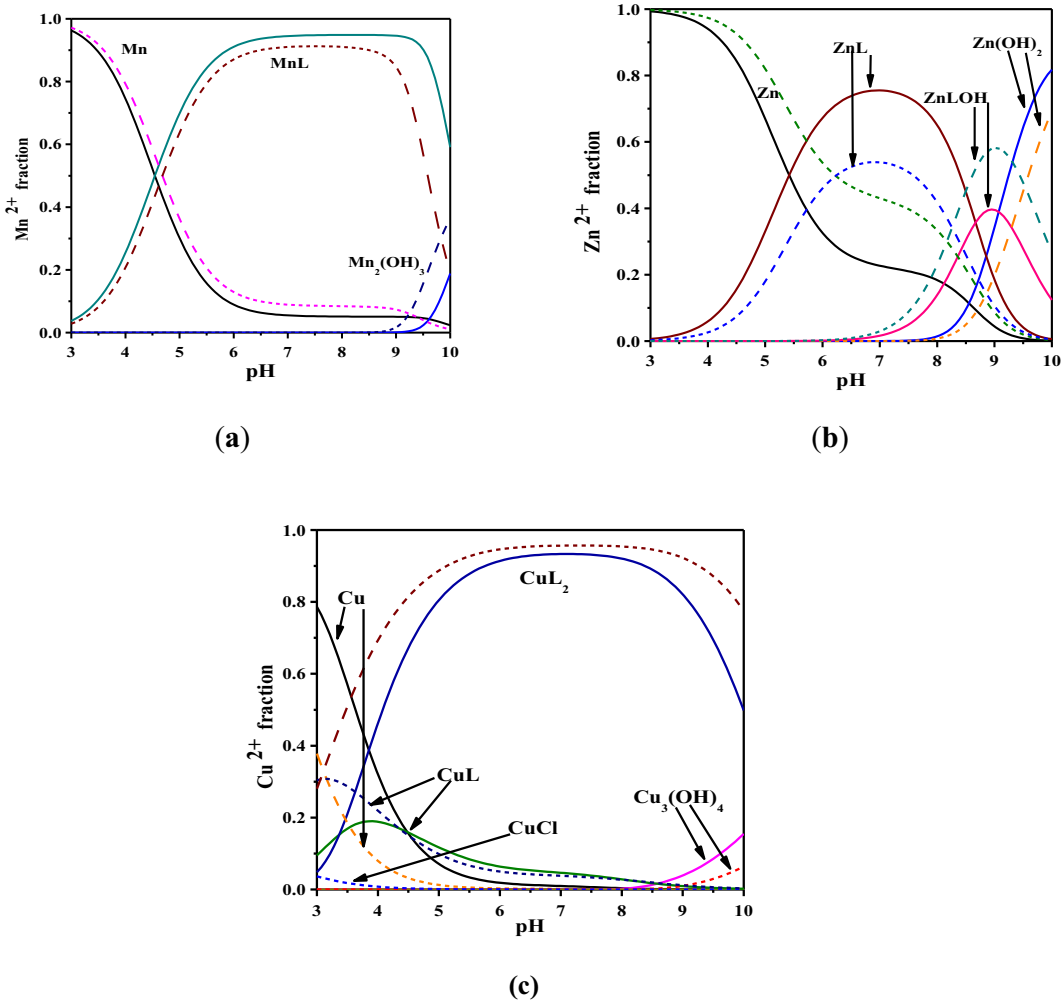

Fig. 3. Speciation diagrams of M-**NAL** (L) systems at t = 25 °C (solid lines) and t = 37 °C (dotted lines). (a) M = Mn^{2+}; (b) M = Zn^{2+}, (c) M = Cu^{2+}. Experimental conditions: C_L = 2 mmol L^{-1}, C_M = 1 mmol L^{-1}, I = 0.15 mol L^{-1} in NaCl.

investigation without precipitation taking place. This has made it possible to use potentiometry as well as spectrophotometry in the study of the complex formation. To choose the most reliable speciation model and to calculate formation constant values of metal-ligand complexes, titrations were performed on solutions with different metal-ligand ratios.

The equilibrium reactions associated with the formation constant values are the following:

$$M^{2+} + pL^{-} = ML_p^{(2-p)}\ \beta^{MLp} \quad (2)$$

$$M^{2+} + L^{-} + H_2O = MLOH^0 + H^+\ \beta^{MLOH} \quad (3)$$

For the three systems, the best speciation models, common to all temperature and ionic strength conditions, were selected based on different criteria, which consider species formation percentages, simplicity of the model, and the parameters of mean and standard deviation on the fit. Table 2 shows the experimental formation constants values of complex species under different temperature and ionic strength conditions. For Zn^{2+}-L and Mn^{2+}-L systems, under the experimental conditions employed in the potentiometric and spectrophotometric titrations, the species with 1:2 stoichiometry have not reached significant formation percentages to allow their refinement, despite having also used an excess of ligand in the potentiometric measurements. Moreover, the desorption/ionization processes of the MALDI MS technique can give rise to a variation in the composition of the gaseous phase with respect to the solution. On the other hand, the Cu^{2+}-L system shows high percentages of formation of the CuL_2 species under the experimental potentiometric conditions.

For Mn^{2+}-L system, a very simple model has been proposed which provides only MnL species. As reported in Fig. 3a, at $t = 25$ °C and $I = 0.15$ mol L^{-1} it is present in all pH range reaching a Mn^{2+} fraction of 0.9 in the range $6 \leq pH \leq 9.5$. It is also possible to observe that with the increasing of the temperature from 25 to 37 °C the fraction of the ML species decreases.

The speciation profile of Zn^{2+}-L system, evidenced in Fig. 3b, includes the presence of the ZnL and ZnLOH species. More in detail, at $t = 25$ °C and $I = 0.15$ mol L^{-1}, ZnL is the predominant species in the range of $4 \leq pH \leq 8.5$ with a maximum fraction corresponding to almost 0.8 at

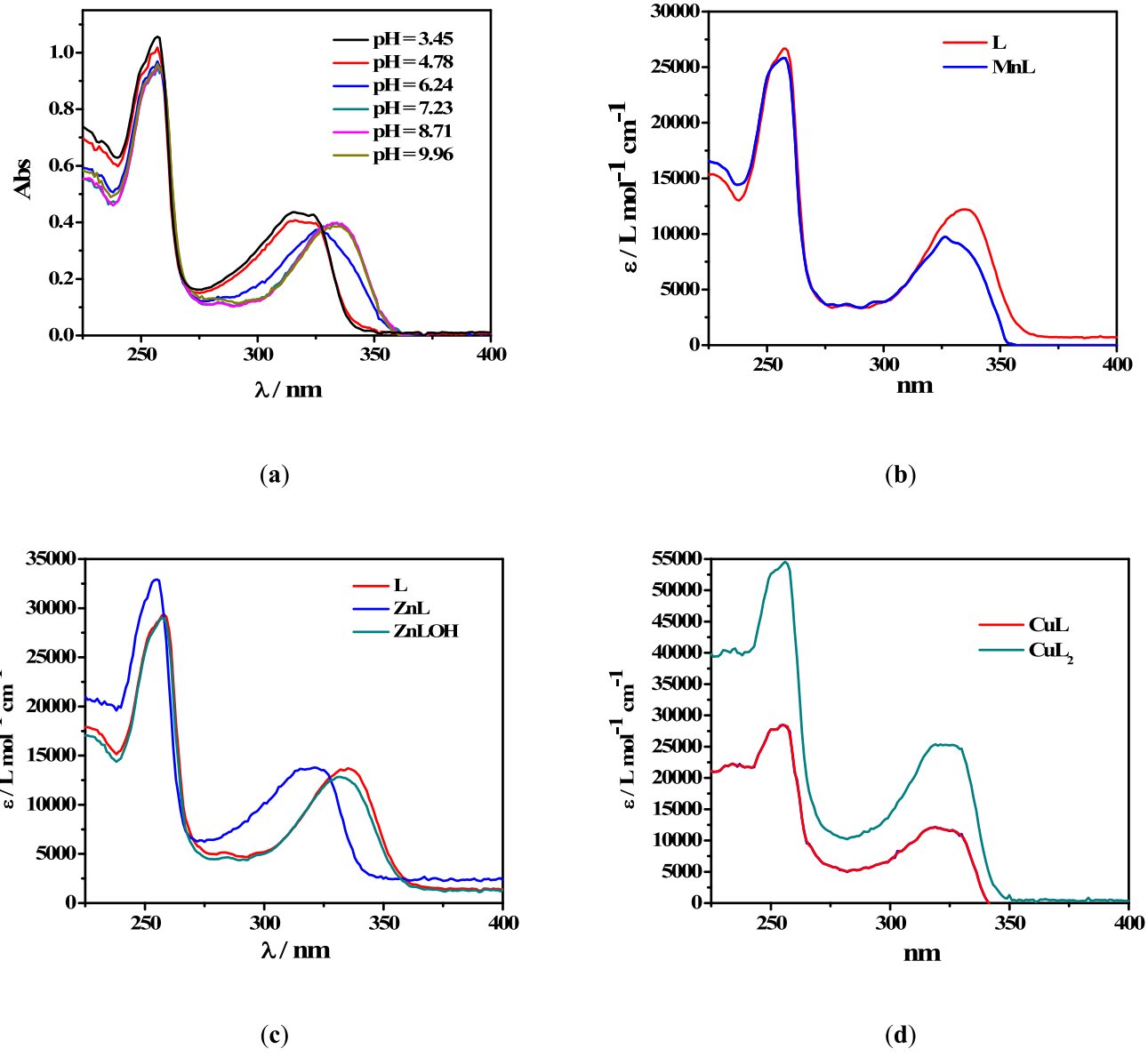

Fig. 4. (a) UV spectra of Mn^{2+}-**NAL** (L) at selected pH values at $C_{Mn} = 0.03$ mmol L^{-1} and $C_L = 0.03$ mmol L^{-1}; (b) ε vs. λ of Mn^{2+}-L species; (c) ε vs. λ of Zn^{2+}-L species, (d) ε vs. λ of Cu^{2+}-L species. Experimental conditions: $t = 25$ °C and $I = 0.15$ mol L^{-1}.

pH = 7, while ZnLOH species prevails at pH = 9 with a maximum of 0.4. The stability and therefore the fractions undergo significant variations by increasing the temperature from 25 °C to 37 °C. It is possible to observe a decrease in the fraction of the ZnL species and an increase of ZnLOH.

For Cu^{2+}-L system the best speciation model provides the formation of CuL and CuL_2 species, whose constant values are reported in Table 2. In Fig. 2 is shown a comparison of speciation diagrams at $t = 25$ °C and $t = 37$ °C. More in detail, CuL is present with low Cu^{2+} fractions in the range of $3 \leq pH \leq 8$, reaching a maximum corresponding to 0.2 at pH = 4, $t = 25$ °C, $I = 0.15$ mol L^{-1}, and 0.3 at $t = 37$ °C. On the contrary, CuL_2 species at $t = 25$ °C reaches a maximum of 0.9 in the range of $6 \leq pH \leq 8.5$, which further increases at $t = 37$ °C.

Various spectrophotometric titrations on solutions containing M-L were performed to study the spectral behavior of complex species and to confirm the formation constant values and the speciation model obtained by potentiometry, as already reported for many other systems [48,49]. The spectrophotometric results showed a fairly good agreement with the potentiometric ones, especially for MnL species (Table S4 of Supplementary Material). The formation constant value of ZnLOH and CuL species, obtained by potentiometry, has been kept constant in the processing of UV data as its low levels of formation are not sufficient for constant refinement.

Fig. 4a shows, by way of example, some of the spectra acquired on solutions containing Mn^{2+}-L at selected pH in the spectral range $225 \leq \lambda \leq 400$ nm. The spectra referred to Zn^{2+}-L system in the same spectral range and pH, reported in the Supplementary Material, show a very similar behavior. The same bathochromic and hypochromic effects as well as the isosbestic point found for L solutions, are visible in the spectra referring to M-L species here reported. Figs. 4b-c show the behavior of the molar extinction coefficients with respect to λ. In Fig. 4b is visible the ε trend of the ML species of the Mn^{2+}-**NAL** system, which reaches two maximum peaks corresponding to 27,000 and 10,000 L mol^{-1} cm^{-1} at λ = 250 and 320 nm, respectively. The ε trend of the ZnL and ZnLOH species (Fig. 4c), shows two maximum peaks, corresponding to 32,500 and 12,500 L mol^{-1} cm^{-1} at λ = 250 and 320 nm for ML species, 30,000 and 11,000 L mol^{-1} cm^{-1} at λ = 260 and 330 nm for MLOH species. The ε trend of the two species of Cu^{2+}-L system, in Fig. 4d, highlights two maximums corresponding to 50,000, 22,500 L mol^{-1} cm^{-1} at λ = 260, 330 nm for ML species, 55,000, 25,000 L mol^{-1} cm^{-1} at λ = 250, 320 nm for ML_2. For data processing, the absorption of Cu^{2+} hydrolytic species was taken into account, considering the ε values obtained in a previous study [49].

3.2. Mn^{2+}-, Zn^{2+}- and Cu^{2+}-**NAL** species under serum conditions

A simulation under real conditions was reported in Fig. 5 to show the relevance of the investigated species. Identifying the presence of complex species and their formation percentage in physiological conditions can be an intriguing topic to examine as the drug complexation could significantly affect its cytotoxicity. **NAL** and the most significant electrolytes in the serum, and their respective equilibria were considered under serum conditions ($t = 37$ °C, $I = 0.15$ mol L^{-1}, $C_{Zn} = 0.02$ mmol L^{-1}, $C_{Cu} = 0.017$ mmol L^{-1},$C_{Mn} = 0.012$ mmol L^{-1}, $C_{NAL} = 0.056$ mmol L^{-1}, $C_{Na} = 140$ mmol L^{-1}, $C_K = 4.3$ mmol L^{-1}, $C_{Ca} = 1$ mmol L^{-1}, $C_{Mg} = 1$ mmol L^{-1}, $C_{Cl} = 102$ mmol L^{-1}, $C_{HCO3} = 21$ mmol L^{-1}, $C_{PO4} = 0.4$ mmol L^{-1}). Ca^{2+} and Mg^{2+}complexes were taken into account by considering literature data ($\log\beta_{CaL} = 2.2$, $\log\beta_{MgL} = 3.0$, $\log\beta_{MgL2} = 5.95$, $\log\beta_{MgLOH} = -4.65$) [50]. Under the serological pH conditions, it is possible to remark that the CuL_2 complex species is the predominant one, reaching a formation percentage of 49%, followed by MgL (15%), MgLOH (10%), CuL (5%) and MnL (4%) species. This simulation underlines the importance of the study of the dependence of the formation constant on temperature and ionic strength to predict the behavior of the species under real conditions. The interaction between Cu^{2+} and L under physiological conditions proves to be almost considerable.

3.3. Dependence of protonation and formation constants on ionic strength and temperature

Protonation and formation constants are significantly influenced by temperature and ionic strength parameters. For this reason, the determination of constants under different conditions of ionic strength is crucial to simulate the real conditions of real fluids. By carrying out the measurements at different ionic strengths, it is possible to study the dependence of the protonation and formation constants on this parameter, applying the following Debye-Hückel type equation applied in several previous papers [51]:

$$\log\beta = \log\beta^0 - 0.51z^* \frac{\sqrt{I}}{1 + 1.5\sqrt{I}} + CI \quad (4)$$

where β^0 is the protonation constant at infinite dilution, z* is the parameter that refers to the charges of the species involved in the formation equilibrium, i.e. $\sum z^2$reagents - $\sum z^2$products, and C is an empirical parameter that depends on the stoichiometric coefficients and on charges. The formation constants extrapolated to $I = 0$ mol L^{-1}, together with C values are summarized in Table 3. The knowledge of

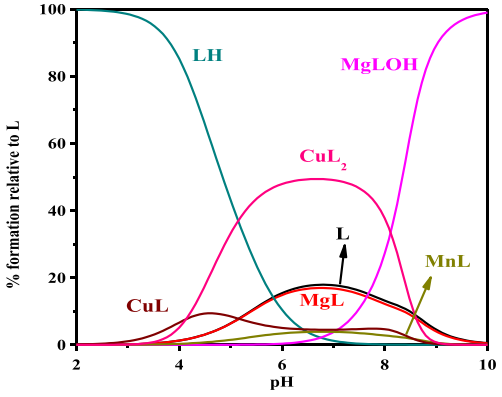

(a)

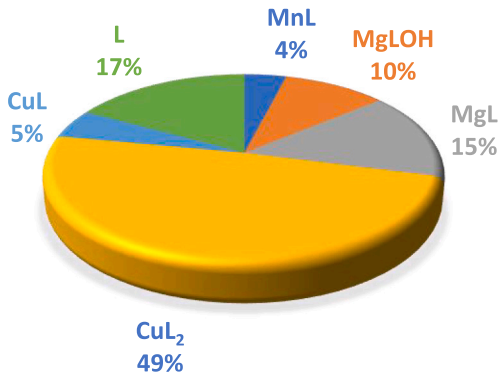

(b)

Fig. 5. (a) Speciation diagram of **NAL** in the presence of the serum main elelectrolytes vs. pH under serum conditions; (b) pie diagram at pH = 7.4. Conditions: $C_{Cu} = 0.017$ mmol L^{-1}, $C_{Zn} = 0.02$ mmol L^{-1}, $C_{Mn} = 0.024$ mmol L^{-1}, $C_{NAL} = 0.056$ mmol L^{-1}, $C_{Na} = 140$ mmol L^{-1}, $C_K = 4.3$ mmol L^{-1}; $C_{Ca} = 1$ mmol L^{-1},$C_{Mg} = 1$ mmol L^{-1}, $C_{Cl} = 102$ mmol L^{-1}, $C_{HCO3} = 21$ mmol L^{-1}, $C_{PO4} = 0.4$ mmol L^{-1}, $t = 37$ °C, $I = 0.15$ mol L^{-1}.

Table 3
Protonation constants at infinite dilution and parameters for the dependence on ionic strength (eq. (4)), of **NAL** (L) and M-L species at $t = 25$ °C in NaCl.

Reaction [1]	logβ^0	C
L+ H = LH	6.22(1)[2]	−0.11(1)[2]
Zn + L = ZnL	3.7(2)	0.5(2)
Zn + L + H_2O = ZnLOH + H	−5.3(1)	1.1(2)
Mn + L = MnL	4.7(1)	0.8(2)
Cu + L = CuL	5.6(1)	0.6(2)
Cu + 2 L = CuL_2	11.06(9)	−0.5(1)

[1] Charges omitted for simplicity; [2] ≥ 95% of confidence interval.

these parameters made it possible to calculate logβ values at the specific ionic strength of a biological fluid.

The determination of the protonation and formation constants at different temperatures allows to study the dependence of the constant values on this parameter, and therefore indirectly, to calculate the protonation and formation enthalpies change values. The protonation and formation constants were processed using the following van't Hoff equation, employed for many other systems [40,52]:

$$\log\beta_T = \log\beta_\theta + \Delta H^0\left(\frac{1}{\theta} - \frac{1}{T}\right) R\ ln\ 10 \quad (5)$$

where $\log\beta_T$ is the stability constant at a certain temperature (expressed in kelvin), while $\log\beta_\theta$ is the stability constant at $t = 298.15$ K, and R is the universal gas constant expressed as 8.314 J K^{-1} mol^{-1}. The values of formation enthalpy changes of all the species of Mn^{2+}-L and Zn^{2+}-L systems are collected in Table 4, together with entropy and free energy change values. It is possible to note an exothermic formation enthalpy change for ZnL and MnL species. The protonation equilibrium is also characterized by an exothermic enthalpy change value. An endothermic trend has been obtained for CuL and CuL_2 species, where the formation entropy change gives the greatest contribution to the Gibbs free energy change, typical of electrostatic interactions. The bar plot of the thermodynamic parameters referred to M-**NAL** species at $t = 25$ °C and $I = 0.15$ mol L^{-1} in NaCl is reported in Fig. S3 of Supplementary Material. The calculated protonation constants of **NAL** (L) and formation constants of Zn^{2+}-L, Mn^{2+}-L, and Cu^{2+}-L species, obtained fitting experimental constant values of Table 2 by considering eqs. (4) and (5), are listed in Table S6 of Supplementary Material.

3.4. Sequestering ability

The sequestering ability represents the tendency of a ligand to complex a free metal cation in solution, forming metal-ligand species. It, therefore, allows to define the capacity of a ligand to decrease the concentration of a free cation in solution. To describe the sequestering ability of a ligand towards a certain metal cation, however, the mere knowledge of formation constants is not sufficient, because it is necessary to consider all the possible interactions that both ligand and metal cation can have with the species present in solution. In order to define it quantitatively, the empirical parameter $pL_{0.5}$ was introduced, which represents the cologarithm of the ligand concentration necessary to sequester 50% of the metal cation in traces, widely used on various systems [53–55]. The calculation is based on the following Boltzmann-type sigmoidal equation:

$$\chi = \frac{1}{1 + 10^{(pL - pL_{0.5})}} \quad (6)$$

where χ is the sum of molar fractions of the different complex species and pL is the co-logarithm of the total ligand concentration. To evaluate the sequestering ability of L towards Mn^{2+}, Zn^2, and Cu^{2+}, $pL_{0.5}$ values were calculated under different pH values and temperatures. According to the calculated $pL_{0.5}$values at $t = 37$ °C, $I = 0.15$ mol L^{-1} and pH plasma mean value (pH = 7.4), the order of sequestering ability is the following, as evidenced in the Fig. S4 in Supplementary Material:

$$pL_{0.5}\left(Cu^{2+}\right)\rangle\ pL_{0.5}\left(Mn^{2+}\right)\rangle\ pL_{0.5}\left(Zn^{2+}\right)$$

Table 4
ΔG, ΔH, $T\Delta S$ of **NAL** (L) and M-L species at $t = 25$ °C and $I = 0.15$ mol L^{-1} in NaCl.

Reaction[1]	ΔG^2	ΔH^2	$T\Delta S^2$
L+ H = LH	−34	−16(1)[3]	18
Zn + L = ZnL	−20	−15(5)	5
Zn + L + H_2O = ZnLOH + H	30	31(8)	1
Mn + L = MnL	−24	−31(2)	−7
Cu + L = CuL	−29	3(7)	32
Cu + 2 L = CuL_2	−58	84(6)	142

[1] Charges omitted for simplicity; [2] Expressed in kJ mol^{-1}; [3] ≥ 95% of confidence interval.

3.5. Mass spectrometry analysis

It is generally accepted that MALDI mass spectra qualitatively reflect the amount of pre-formed complexes between metal ions and analytes or MALDI matrices in the solid sample. Matrix is generally a laser-absorbing small molecule; thus, it is reasonable to test whether the analyte can be analyzed without a matrix. The mass spectra acquired without an external matrix would be simple, and the signal variability would be reduced due to more homogeneity in the formed crystals. Also, the monitoring of the interaction between metal ions and analyte would be more reliable. However, it is reported that the highly charged clusters of matrices induced by laser irradiation are expanded into the plume, and undergo charge reductions to the states of one and zero by neutralization with electrons or matrix anions in positive mode [21,56–58]. Although pre-formed ions play an important role in the case of metal ion–matrix complexes it has to be considered that if more energy is transferred to the ion pairs, the proton transfer from the positive sites to the anions can be enhanced. Thus, only the complexes between metal ions and analytes or matrices surviving the ionization processes can then be detected and analyzed with the mass spectrometer. It has to be considered that the exact position of the metal ions relative to the analyte molecules in the matrix crystal is unknown, the distance between ion pairs can be influenced by solvation or hydrogen bonds [59,60] and that matrix anions can compete for positive sites with anions added to or present in the solution [61,62]. Therefore, **NAL** will be initially checked for its ability to show up in the LD-MS and reveal the expected ion species ([M, **NAL**]$^+$, [M, 2**NAL**]$^+$, [2(M,2**NAL**)]$^+$) for all cations without an external matrix. In the case of Mn, Zn, Cu /**NAL** systems, the expected species, and plausible structures will be reported. The complexation behavior of **NAL** towards metal ions may qualitatively reflect the amount of metal/**NAL** pre-formed complexes, the cation absorption into **NAL** crystal as well as the energetics of the ionization/desorption and release of the ion species. All these processes are in turn strictly correlated to the nature of metal cations. The first step was to analyze by LDMS the free **NAL** to elucidate its gas phase ion chemistry behavior. It is well known that **NAL** is able to form hydrogen bounding networks, in particular its quinolone structure seems to be responsible of interaction with DNA and other nucleic acids [56,63,64]. These interactions are deeply influenced by the formation of hydrogen bonding that have manifold possibilities of donor acceptor group-interaction between **NAL** and DNA-helix, but also between **NAL** units. Furthermore, literature data report the dimerization process of quinolones by mass spectrometry, also in presence of metal cations [31,65]. Spectrum reported in Fig. 6 shows the presence of ions proving information on different protonated species, that are identified by the distribution of the signals and are listed in Table 5. The spectrum shows the formation of three clusters regions ascribable to three, two and one units of **NAL** linked together.

The comparison of the measured experimental isotopic distribution

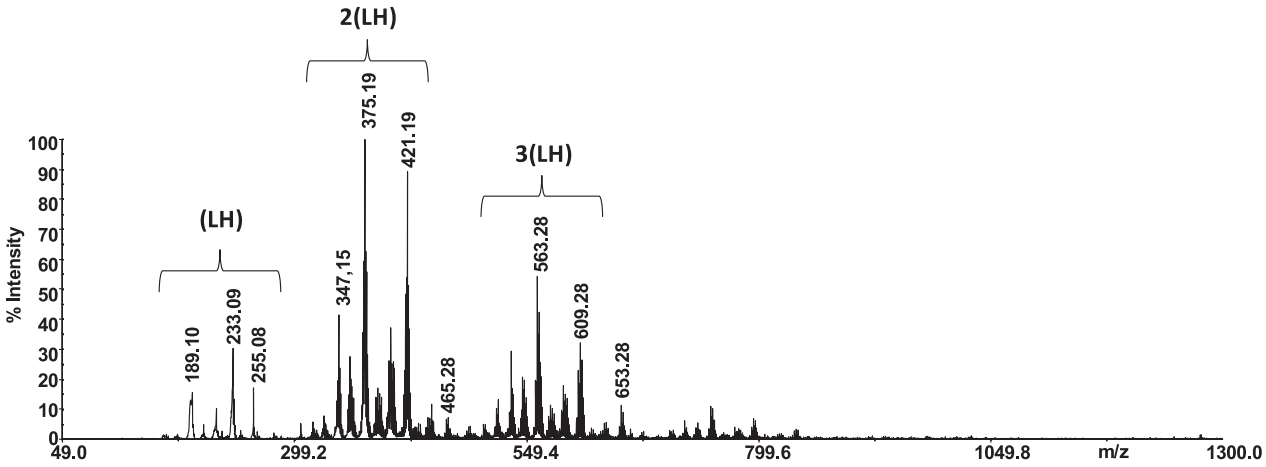

Fig. 6. LD-MS of NAL.

Table 5
MS ions of **NAL** (LH).

Exact mass	Observed *m/z*	Δ(ppm)	Formula	Identified species
653.2718	653.28	5.0	$[C_{35}H_{37}N_6O_7]^+$	$[3(LH)-CO_2+H]^+$
609.2820	609.28	4.5	$[C_{34}H_{37}N_6O_5]^+$	$[3(LH)-2(CO_2)+H]^+$
607.2663	607.27	4.3	$[C_{34}H_{35}N_6O_5$	$[3(LH)-(CO_2)-(HCO_2H)+H]^+$
563.2765	563.28	4.0	$[C_{33}H_{35}N_6O_3]^+$	$[3(LH)-2(CO_2)-(HCO_2H)+H]^+$
465.1769	465.18	3.9	$[C_{24}H_{25}N_4O_6]^+$	$[2(LH)+H]^+$
421.1870	421.19	4.1	$[C_{23}H_{25}N_4O_4]^+$	$[2(LH)-(CO_2)+H]^+$
375.1816	375.18	5.0	$[C_{22}H_{23}N_4O_2]^+$	$[2(LH)-(CO_2)-(HCO_2H)+H]^+$
347.1503	347.15	5.2	$[C_{20}H_{19}N_4O_2]^+$	$[2(LH)-(CO_2)-(HCO_2H)-(28)+H]^+$
255.0740	255.08	4.0	$[C_{12}H_{12}N_2O_3Na]^+$	$[LNa+H]^+$
233.0921	233.09	4.5	$[C_{12}H_{13}N_2O_3]^+$	$[LH+H]^+$
189.1022	189.10	4.6	$[C_{11}H_{13}N_2O]^+$	$[LH-(CO_2)+H]^+$

with the theoretically calculated distribution of the expected summary formula, suggests that the ion clusters of *m/z* 233.09 ($[C_{12}H_{13}N_2O_3]^+$, $[LH+H]^+$) and 465.18 ($[C_{24}H_{25}N_4O_6]^+$, $[2(LH)+H]^+$) correspond to one and two **NAL** units, respectively. The ion of m/z 653.28 arises from the loss of 44 Da (CO_2) from three **NAL** units ($[C_{35}H_{37}N_6O_7]^+$, $[3(LH)-CO_2+H]^+$). Several of the observed ion species arise from the loss of 44 (CO_2) and 46 (HCOOH) leading to the formation of the ion species reported in Table 5. The structures of **NAL** clusters show evident stability in the adopted experimental conditions, and the understanding of them is important to investigate the effect of the presence of different counterions influencing intermolecular interactions.

The structures of Zn^{2+} and Mn^{2+}complex species with **NAL** are investigated by laser desorption mass spectrometry (LDMS). Fig. 7 shows the LD-MS spectra of complexes [LH, Zn^{2+}] and [LH, Mn^{2+}]. The divalent cations are chelated by the ligand and the formation of species with stoichiometry 1:2 (metal: ligand) is favored under the adopted experimental conditions. All the species are identified by the comparison of the high-resolution mass to charge (*m/z*) values and the theoretical isotopic distribution. The spectrum reported in Fig. 7a shows the formation of signals of *m/z* 549.07, 505.09 and 461.09. The first is

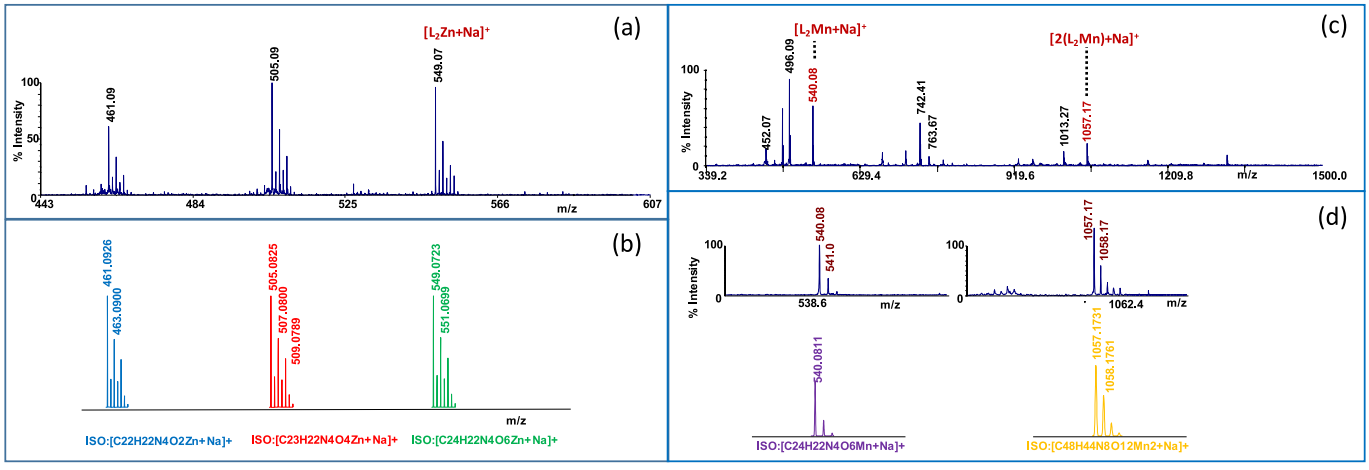

Fig. 7. LD-MS (a) and theoretical distribution of the isotope cluster ions (b) of Zn^{2+}-**NAL** complex; LD-MS (c) and theoretical distribution of the isotope cluster ions (d) of Mn^{2+}-**NAL** complex.

ascribable to the sodiated complex Zn^{2+}-**NAL** with (1:2) stoichiometry $[L_2Zn + Na]^+$ ($[C_{24}H_{22}N_4O_6Zn + Na]^+$, *m/z* 549.07), while the others are deriving from the two consecutive loss of 44 Da from *m/z* 549.07 ion (m/z 505.09,$[C_{23}H_{22}N_4O_4Zn + Na]^+$; m/z 461.09, $[C_{22}H_{22}N_4O_2Zn + Na]^+$). The comparison between the theoretically calculated distribution of the expected formula (Fig. 7b) and the measured experimental isotopic distribution corroborates the elemental formula and confirms the formation of the complex with 1:2 (metal:ligand) stoichiometry. The spectrum depicted in Fig. 7c substantiates comparable information regarding Mn^{2+}-**NAL** complex. The ion species of *m/z* 540.08 ($[C_{24}H_{22}N_4O_6Mn + Na]^+$) corresponding to the sodiated complex with 1:2 (metal:ligand) stoichiometry confirms the isotopic distribution and elemental formula (Fig. 7d). The ion species of *m/z* 1057.18 (Fig. 7c) corresponds to the sodiated dimeric cluster $[2(L_2Mn + Na]^+]$ ($[C_{48}H_{44}N_8O_{12}Mn_2 + Na]^+$) containing two Mn^{2+} and four deprotonated ligands, as confirmed by the theoretically calculated distribution of the expected summary formula (Fig. 7d).

Tandem mass spectrometry experiments were performed in order to assign the metal coordination sites of the observed complexes. MS/MS experiments were recorded, both for the complexes [LH, Zn^{2+}] and [LH, Mn^{2+}] with 1:2 (metal: ligand) stoichiometry. The MS/MS spectrum of the ionic species of m/z 549.07 ($[C_{24}H_{22}N_4O_6Zn + Na]^+$) showed an extensive fragmentation of the precursor (Fig. 8a and Table 6), displaying ion peaks arising from the direct and consecutive fragmentation pathways.

The direct and consecutive neutral losses of 44 (m/z 505.9, $[C_{23}H_{22}N_4O_4Zn + Na]^+$; m/z 461.09 $[C_{22}H_{22}N_4O_2Zn + Na]^+$) from ML_2 suggest the good stability of the metal complex. The formation of the sodiated ion of *m/z* 319.01 ($[C_{12}H_{12}N_2O_3Zn + Na]^+$) arises from the loss of an integer ligand. Results indicate that the deprotonated ligands coordinate Zn^{2+}via oxygen atom of the carboxylate moiety with the assistance of the carbonyl group oxygen [64]. Similar fragmentation patterns have been observed in MS/MS spectrum of the ion of m/z 540.08 ($[C_{24}H_{22}N_4O_6Mn + Na]^+$,Fig. 8b) regarding Mn^{2+}-**NAL** complex with 1:2 (metal:ligand) stoichiometry. However, the signal intensities of fragment ions are not very significant, except for the first ion of m/z 496.09 arising from the neutral loss of 44 Da.

All observed fragments contain the metal cation, signifying a stable Mn^{2+} coordination, and also in this case is observed the formation of the sodiated ion of m/z 309.01 ($[C_{12}H_{11}N_2O_3Mn + Na]^+$) arising from the loss of an integer ligand. For the dimeric complex, the ligands underwent dissociation of their structures upon MS/MS conditions, but only few non-informative fragments are occurring (Supplementary Material, Fig. S5).

NAL structure allows the formation of stable complexes with both Zn^{2+} and Mn^{2+}*via* adjacent carboxylic and ketone groups. The formation of complex species was observed for both cations. MS/MS spectra of metal-ligand species showed few structurally diagnostic fragment ions, that related to Zn^{2+} complex provide more useful information for the structural characterization than that from Mn^{2+} complexes.

The coordination of copper is quite similar. Also in this case, all species are identified by the characteristic distribution of copper

Table 6
LD MS and MS/MS fragments of [LH, Zn^{2+}] and [LH, Mn^{2+}] complexes (LH = **NAL**).

	Composition	Detected Mass	Δ(ppm)
$[L_2Zn + Na]^+$	$[C_{24}H_{22}N_4O_6Zn + Na]^+$	549.07	5.0
MS/MS fragments	$[C_{23}H_{22}N_4O_4Zn + Na]^+$	505.09	8.0
	$[C_{22}H_{22}N_4O_2Zn + Na]^+$	461.09	6.0
	$[C_{12}H_{12}N_2O_3Zn + Na]^+$	319.01	6.0
	$[C_{10}H_{10}N_2O_2Zn + Na]^+$	276.99	8.0
	$[C_{10}H_8N_2O_2 + Na]^+$	211.05	7.5
$[L_2Mn + Na]^+$	$[C_{24}H_{22}N_4O_6Mn + Na]^+$	540.08	5.0
$[2(L_2Mn) + Na]^+$	$[C_{48}H_{44}N_8O_{12}Mn_2 + Na]^+$	1057.18	4.5
MS/MS fragments	$[C_{23}H_{22}N_4O_4Mn + Na]^+$	496.09	5.0
	$[C_{22}H_{22}N_4O_2Mn + Na]^+$	452.10	6.5
	$[C_{19}H_{14}N_4O_3Mn + Na]^+$	424.04	6.0
	$[C_{12}H_{11}N_2O_3Mn + Na]^+$	309.01	7.0
	$[C_{11}H_{11}N_2OMn]^+$	242.03	6.5
	$[C_9H_7N_2OMn]^+$	213.99	6.0

Table 7
LD MS of [LH, Cu^{2+}]; (LH = **NAL**).

Exact mass	Observed m/z	Δ(ppm)	Formula	Identified species
548.07	548.08	5.0	$[C_{24}H_{22}N_4O_6CuNa]^+$	$[CuL_2 + Na]^+$
526.09	526.10	6.5	$[C_{24}H_{23}N_4O_6Cu]^+$	$[CuL_2 + H]^+$

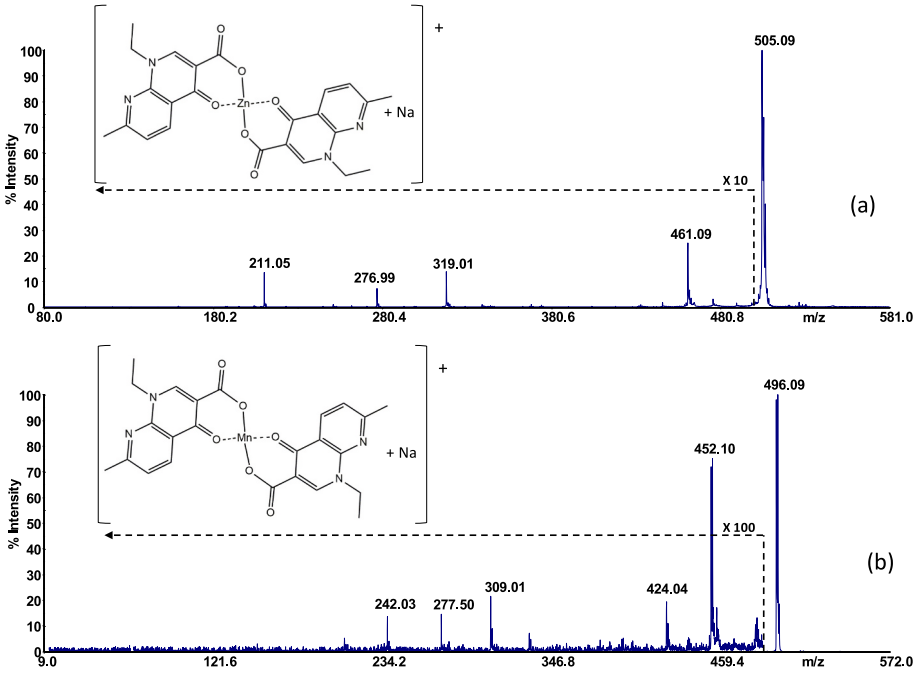

Fig. 8. MS/MS spectra of the complexes: (a) $[L_2Zn + Na]^+$, *m/z* 549.07; (b) $[L_2Mn + Na]^+$, m/z 540.08.

isotopes, the comparison of the high-resolution mass to charge (*m/z*) values and the theoretical isotopic distribution (Table 7). The mass-to-charge (m/z) values refer to complex with metal-ligand 1:2 stoichiometry, even if signals intensities are very weak. In order to preserve the complex structure, different experiments were performed using traditional MALDI (matrix assisted laser desorption ionization) matrices. Unfortunately, alpha-cyano-4-hydroxy-cinnamic acid (α-CHCA) and 2,5-dihydroxybenzoic acid (DHB) compete with **NAL** for the metal coordination, resulting in loss of information about Cu^{2+} coordination sites.

Tandem mass spectrometry experiments were performed to clarify the copper coordination sites. For the complex with 1:2 stoichiometry, the ligands underwent dissociation, but only few non-informative fragments are observed. All observed fragments contain the metal cation, index of a stable Cu^{2+} coordination. In addition, it is observed the formation of the sodiated ion of m/z 316.99 ($[C_{12}H_{11}N_2O_3Cu + Na]^+$) arising from the loss of an integer ligand.

3.6. Comparison with literature data

Few protonation constant data of **NAL** as well as formation constant values with Mn^{2+} and Zn^{2+} are present in the literature and in the most used databases. No systematic study at different temperatures and ion strengths was performed. There are only few data at a single value of ionic strength and temperature. Among them, a protonation constant value of $\log K_1 = 5.943$ at $t = 37$ °C and $I = 0.15$ mol L^{-1} in NaCl was reported in the papers [63,64]. This value is in good agreement with the one here reported ($\log K_1 = 5.82$) under the same conditions of temperature, ionic strength, and ionic medium (see Table 2). The protonation constant reported by Huang et al., corresponding to $\log K_1 = 5.94$, at $t = 37$ °C and $I = 0.15$ mol L^{-1} in NaCl, is also very close to the value here reported [50,65]. One paper reports the formation constants of Zn^{2+}-**NAL** and Mn^{2+}-**NAL** species, but it is dated and therefore affected by a series of major limitations both from the point of view of the experimental method and of data processing. Therefore, the results of the paper [31] are not comparable with those here reported. Formation constant values for Cu^{2+}-**NAL** interaction were proposed as $\log\beta_1 = 6.0$ and $\log\beta_2 = 11.64$, for ML and ML_2 species, respectively, at $t = 37$ °C and $I = 0.15$ mol L^{-1} in NaCl [31,66,67]. These values are fairly close to the ones here reported in NaCl under the same conditions ($\log\beta_1 = 5.68$, $\log\beta_2 = 11.42$, see Table 2).

4. Conclusion

This work had as main objective the elucidation of behavior of **NAL** in aqueous solution and of its interaction with Zn^{2+}, Mn^{2+} and Cu^{2+} to better understand the influence of complexation on **NAL** efficiency. With this purpose, a combination of potentiometry, UV spectrophotometry, MS and MS/MS investigations were employed to determine the protonation constants, the formation constants with Zn^{2+}, Mn^{2+}, and Cu^{2+} under different conditions, the sequestering ability of **NAL** towards metal cations, the protonation and formation enthalpic and entropic changes, and to assign the ligand coordination sites. The relevance of the systems under study were evaluated calculating the speciation diagram of **NAL** complex species under serum conditions. The results of this simulation showed that the CuL_2 species reaches a significant formation percentage under these conditions. Mass spectrometry results allowed to obtain interesting information regarding the formation of complexes. The LD-MS spectra of **NAL** complexes with Zn^{2+} and Mn^{2+} indicate that the divalent cations are chelated via the oxygen atom of the carboxylate moiety with the assistance of the carbonyl group oxygen and the formation of species with 1:2 (metal: ligand) stoichiometry are favored under the experimental conditions of MS experiments. For the manganese complex is also observed the formation of a dimeric species, according to literature data. For the Cu^{2+} system, **NAL** chelates the metal cation in the same manner and fills the metal coordination sphere with two ligands. The MS results confirm the formation of the complexes between Zn^{2+}, Mn^{2+}, Cu^{2+} and **NAL** adding important information on the mode of interaction. The obtained outcomes demonstrate how the complexation of **NAL** with the three metal cations Mn^{2+}, Zn^{2+} and Cu^{2+} can be exploited in order to get alternative liposomal formulations of **NAL**. Particularly, it was demonstrated how the use of the physiological pH (pH = 7.4, generally used in liposomal formulations based on PBS, saline phosphate buffer), the 1:2 metal-L molar ratio and the temperature of 25 °C for Zn^{2+}-L system and 37 °C for Mn^{2+}-L and Cu^{2+}-L systems allow to maximize the interaction with a consequent increase on the formation percentages of the complex species. These preliminary results are valuable for the development of novel liposomal formulations of **NAL**.

Author contributions

Conceptualization, O.G., F·C.; methodology, O.G., F.C.; validation, O.G., F.C., C.F., D.A., A.N.; investigation, F.C., D.A.; data curation, O.G., F.C, D.A.; writing-original draft preparation, O.G, F.C., D.A., A.N.; writing-review and editing, O.G., C.F., A.N.; supervision, O.G., A.N. All authors have read and agreed to the published version of the manuscript.

Funding

This research did not receive any specific grant from funding agencies in the public, commercial, or not-for-profit sectors.

Author statement

The authors declare the availability of the data reported in this paper.

Declaration of Competing Interest

The authors declare no conflict of interest.

Data availability

Data will be made available on request.

Appendix A. Supplementary data

Supplementary data to this article can be found online at https://doi.org/10.1016/j.jinorgbio.2023.112366.

References

[1] S. Sengupta, M.K. Chattopadhyay, H.P. Grossart, The multifaceted roles of antibiotics and antibiotic resistance in nature, Front. Microbiol. 4 (2013) 47.
[2] U. Shimanovich, A. Gedanken, Solutions to restore antibiotic activity, J. Mater. Chem. B 4 (2016) 824–833.
[3] V. André, P.C. Alves, M.T. Duarte, Exploring antibiotics as ligands in metal–organic and hydrogen bonding frameworks: our novel approach towards enhanced antimicrobial activity (mini-review), Inorg. Chim. Acta 525 (2021), 120474.
[4] V. André, F. Galego, M. Martins, Mechanochemical assembly of nalidixic acid bioinspired metal–organic compounds and complexes toward improved solubility, Cryst. Growth Des. 18 (2018) 2067–2081.
[5] J.M. Feio, I. Sousa, M. Ferreira, L. Cunha-Silva, R.G. Saraiva, C. Queiros, J. G. Alexandre, V. Claro, A. Mendes, R. Ortiz, S. Lopes, A.L. Amaral, J. Lino, P. Fernandes, A.P. Silva, L. Moutinho, B. de Castro, L. Perello Pereira, P. Gameiro, Fluoroquinolone–metal complexes: a route to counteract bacterial resistance? J. Inorg. Biochem. 138 (2014) 129–143.
[6] J. Davies, D. Davies, Origins and evolution of antibiotic resistance, Microbiol. Mol. Biol. Rev. 74 (2010) 417–433.
[7] R.J. Fair, Y. Tor, Antibiotics and bacterial resistance in the 21st century, Perspect Med. Chem 6 (2014) 25–64.
[8] M. Eddaoudi, D.F. Sava, J.F. Eubank, K. Adil, V. Guillerm, Zeolite-like metal-organic frameworks (ZMOFs): design, synthesis, and properties, Chem. Soc. Rev. 44 (2015) 228–249.

[9] Z. Golkar, O. Bagazra, D.G. Pace, Bacteriophage therapy: a potential solution for the antibiotic resistance crisis, J. Infect. Dev. Ctries. 8 (2014) 129–136.
[10] A. Pandey, N. Aggarwal, A. Adholeya, M. Kochar, Resurrection of nalidixic acid: evaluation of water-based nanoformulations as potential nanomedicine, Nanoscale Res. Lett. 13 (2018) 298.
[11] S. Bouson, A. Krittayavathananon, N. Phattharasupakun, P. Siwayaprahm, M. Sawangphruk, Antifungal activity of water-stable copper-containing metal-organic frameworks, R. Soc. Open Sci. 4 (2017), 170654.
[12] S. Li, F. Huo, Metal-organic framework composites: from fundamentals to applications, Nanoscale. 7 (2015) 7482–7501.
[13] M. Mueller, X. Zhang, Y. Wang, R.A. Fischer, Nanometer- sized titania hosted inside MOF-5, Chem. Commun. 1 (2009) 1007–1026.
[14] C. Abate, F. Carnamucio, O. Giuffrè, C. Foti, Metal-based compounds in antiviral therapy, Biomolecules 12 (2022) 933.
[15] R. Mirzajani, F. Kardani, Z. Ramezani, Preparation and characterization of magnetic metal–organic framework nanocomposite as solid-phase microextraction fibers coupled with high-performance liquid chromatography for determination of non-steroidal anti-inflammatory drugs in biological fluids and tablet formulation samples, Microchem. J. 144 (2019) 25.
[16] S. Rojas, T. Devic, P. Horcajada, Metal organic frameworks based on bioactive components, J. Mater. Chem. B 5 (14) (2017) 2560–2573.
[17] Y. Kawabata, K. Wada, M. Nakatani, S. Yamada, S. Onoue, Formulation design for poorly water-soluble drugs based on biopharmaceutics classification system: basic approaches and practical applications, Int. J. Pharm. 420 (2011) 1–10.
[18] F. Arjmand, I. Yousuf, T.B. Hadda, L. Toupet, Synthesis, crystal structure and antiproliferative activity of Cu(II) nalidixic acid- DACH conjugate: comparative in vitro DNA/RNA binding profile, cleavage activity and molecular docking studies, Eur. J. Med. Chem. 81 (2014) 76–88.
[19] G. Mendoza-Díaz, L.M.R. Martinez-Aguilera, R. Perez-Alonso, X. Solans, R. Moreno-Esparza, Synthesis and characterization of mixed ligand complexes of copper with nalidixic acid and (NN) donors. Crystal structure of [Cu(Phen)(Nal)-(H2O)]NO3•3H2O, Inorg. Chim. Acta 138 (1987) 41–47.
[20] M. Rizk, F. Belal, F.A. Aly, N.M. El-Enany, Fluorimetric determination of nalidixic acid in formulations and biological fluids through ternary complex formation, Anal. Lett. 30 (1997) 1897–1908.
[21] C. Bravo, F. Galego, V. André, Hydrogen bonding networks of nalidixic acid–copper(II) complexes, Cryst. Eng. Comm. 21 (2019) 7199–7203.
[22] M. Kumar, N. Kumar Mogha, G. Kumar, F. Hussain, D.T. Masram, Biological evaluation of copper(II) complex with nalidixic acid and 2,2′- bipyridine (bpy), Inorg. Chim. Acta 490 (2019) 144–154.
[23] F.R.G. Bergaminia, J.H.B. Nunesa, M.A. de Carvalhoc, M.A. Ribeirod, P.P. de Paivae, T.P. Banzatof, A.L.T.G. Ruize, J.E. de Carvalhoe, W.R. Lustrig, D.O.T. A. Martinsh, A.M. da Costa Ferreirah, P.P. Corbi, Polynuclear copper(II) complexes with nalidixic acid hydrazones: antiproliferative activity and selectivity assessment over a panel of tumor cells, Inorg. Chim. Acta 484 (2019) 491–502.
[24] R.M. Gandra, P. Mc Carron, M.F. Fernandes, L.S. Ramos, T.P. Mello, A.C. Aor, M. H. Branquinha, M. McCann, M. Devereux, A.L.S. Santos, Antifungal potential of copper(II), manganese(II) and silver(I) 1,10-phenanthroline chelates against multidrug-resistant fungal species forming the candida haemulonii complex: impact on the planktonic and biofilm lifestyle, Front. Microbiol. 8 (2017) 1257.
[25] I. Iakovidis, I. Delimaris, S.M. Piperakis, Copper and its complexes in medicine: a biochemical approach, Mol. Biol Intern. 2011 (2011), 594529.
[26] R. Loganathana, M. Ganeshpandiana, N.S.P. Bhuvaneshb, M. Palaniandavara, A. Murugananthamc, S.K. Ghoshc, A. Riyasdeend, M.A. Akbarsha, DNA and protein binding, double-strand DNA cleavage and cytotoxicity of mixed ligand copper(II) complexes of the antibacterial drug nalidixic acid, J. Inorg. Biochem. 174 (2017) 1–13.
[27] S. Zakelj, K. Berginc, D. Uršič, M. Veber, A. Kristl, Metal cation–fluoroquinolone complexes do not permeate through the intestinal absorption barrier, J. Pharm. Biomed. Anal. 53 (2010) 655–659.
[28] D.L. Ross, S.K. Elkinton, S.R. Knaub, C.M. Riley, Physicochemical properties of the fluoroquinolone antimicrobials. VI: effects of metal-ion complexation on octan-1-ol-water partitioning, Int. J. Pharm. 93 (1993) 131–138.
[29] F. Arjmand, I. Yousuf, M. Afzal, L. Toupet, Design and synthesis of new Zn(II) nalidixic acid-DACH based topo-II inhibiting molecular entity: chemotherapeutic potential validated by its in vitro binding profile, pBR322 cleavage activity and molecular docking studies with DNA and RNA molecular targets, Inorg. Chim. Acta 421 (2014) 26–37.
[30] R. Gleckman, S. Alvares, D.W. Joubert, S.J. Matthews, Drug therapy reviews: nalidix acid, Am. J. Hosp. Pharm. 36 (1979) 1071–1076.
[31] K. Timmers, R. Sternglanz, Ionization and divalent cation dissociation constants of nalidixic and oxolinic acids, Bioinorg. Chem. 9 (1978) 145–155.
[32] T. Aycan, F. Öztürk, T. Doruk, S. Demir, M. Fidan, H. Paşaoğlu, Synthesis, structural, spectral and antimicrobial activity studies of copper-nalidixic acid complex with 1,10-phenanthroline: DFT and molecular docking, Spectrochim. Acta A Mol. Biomol. Spectrosc. 241 (2020), 118639.
[33] M. Budai, Z. Szabó, A. Zimmer, M. Szögyi, P. Gróf, Studies on molecular interactions between nalidixic acid and liposomes, Int. J. Pharm. 279 (2004) 67–79.
[34] B.C.L. Cheung, T.H.T. Sun, J.M. Leenhouts, P.R. Cullis, Loading of doxorubicin into liposomes by forming Mn^{2+}–drug complexes, Biochim. Biophys. Acta 1414 (1998) 205–2016.
[35] G.N.C. Chiu, S.A.S.A. Abrahama, L.M. Ickensteina, R.N. Goran Karlssond, K. Edwardsd, E.K. Wasana, M.B. Bally, Encapsulation of doxorubicin into thermosensitive liposomes via complexation with the transition metal manganese, J. Control. Release 104 (2005) 271–288.
[36] B.M. Lomaestro, G.R. Bailie, Absorption interactions with fluoroquinolones, Drug Saf. 12 (1995) 314–333.
[37] A. Beneduci, G.A. Corrente, T. Marino, D. Aiello, L. Bartella, L. Di Donna, A. Napoli, N. Russo, I. Romeo, E. Furia, Insight on the chelation of aluminum(III) and iron(III) by curcumin in aqueous solution, J. Mol. Liq. 296 (2019), 111805.
[38] C. Abate, D. Aiello, M. Cordaro, O. Giuffrè, A. Napoli, C. Foti, Binding ability of L-carnosine towards Cu^{2+}, Mn^{2+} and Zn^{2+} in aqueous solution, J. Mol. Liq. 368 (2022), 120772.
[39] E. Furia, R. Porto, 2-Hydroxybenzamide as a ligand. Complex formation with dioxouranium(VI), aluminum(III), neodymium(III), and nickel(II) ions, J. Chem. Eng. Data 53 (2008) 2739–2745.
[40] D. Aiello, M. Cordaro, N. Napoli, F. Foti, G. Giuffrè, Speciation study on O-phosphorylethanolamine and O-phosphorylcholine: acid–base behavior and Mg^{2+} interaction, Front. Chem. 10 (2022), 864648.
[41] D. Taverna, L. Di Donna, F. Mazzotti, A. Tagarelli, A. Napoli, E. Furia, G. Sindona, Rapid discrimination of bergamot essential oil by paper spray mass spectrometry and chemometric analysis: PS-MS and chemometrics of bergamot essential oil, J. Mass Spectrom. 51 (2016) 761–767.
[42] L. Salvatore, N. Gallo, D. Aiello, P. Lunetti, A. Barca, L. Blasi, M. Madaghiele, S. Bettini, G. Giancane, M. Hasan, V. Bo-rovkov, M.L. Natali, L. Campa, L. Valli, L. Capobianco, A. Napoli, A. Sannino, An insight on type I collagen from horse tendon for the manufacture of implantable devices, Int. J. Biol. Macromol. 154 (2020) 291–306.
[43] D. Aiello, C. Siciliano, F. Mazzotti, L.D. Donna, R. Risoluti, A. Napoli, Protein extraction, Enrichment and MALDI MS and MS/MS Analysis from Bitter Orange Leaves (*Citrus Aurantium*) 25 (2020) 1485.
[44] C. De Stefano, S. Sammartano, P. Mineo, C. Rigano, *Computer tools for the speciation of natural fluids*, in: A. Gianguzza, E. Pelizzetti, S. Sammartano (Eds.), *Marine Chemistry - An Environmental Analytical Chemistry Approach*, 1997.
[45] P. Gans, A. Sabatini, A. Vacca, Determination of equilibrium constants from spectrophometric data obtained from solutions of known pH: THE PROGRAM pHab, Ann. Chim. 89 (1999) 45–49.
[46] L. Alderighi, P. Gans, A. Ienco, D. Peters, A. Sabatini, A. Vacca, Hyperquad simulation and speciation (HySS): a utility program for the investigation of equilibria involving soluble and partially soluble species, Coord. Chem. Rev. 184 (1999) 311–318.
[47] I. Turel, The interactions of metal ions with quinolone antibacterial agents, Coord. Chem. Rev. 232 (2002) 27–47.
[48] F. Carnamucio, C. Foti, M. Cordaro, O. Giuffrè, Study on metronidazole acid-base behavior and speciation with Ca^{2+} for potential applications in natural waters, Molecules. 27 (2022) 5394.
[49] O. Giuffrè, D. Aiello, D. Chillè, A. Napoli, C. Foti, Binding ability of arsenate towards Cu^{2+} and Zn^{2+}: thermodynamic behavior and simulation under natural water conditions, Environ Sci Process Impacts 22 (2020) 1731–1742.
[50] A.E. Martell, R.M. Smith, R.J. Motekaitis, Critically Selected Stability Constants of Metal Complexes. Gaithersburg, National Institute of Standard and Technology, NIST, *Gaithersburg*, USA, 2004.
[51] D. Chillè, C. Foti, O. Giuffrè, Thermodynamic parameters for the protonation and the interaction of arsenate with Mg^{2+}, Ca^{2+} and Sr^{2+}: application to natural waters, Chemosphere. 190 (2018) 72–79.
[52] D. Aiello, F. Carnamucio, M. Cordaro, C. Foti, A. Napoli, O. Giuffrè, Ca^{2+} complexation with relevant bioligands in aqueous solution: a speciation study with implications for biological fluids, Front. Chem. 9 (2021), 640219.
[53] D. Chillè, D. Aiello, G.I. Grasso, O. Giuffrè, A. Napoli, C. Sgarlata, C. Foti, Complexation of As(III) by phosphonate ligands in aqueous fluids: thermodynamic behavior, chemical binding forms and sequestering abilities, J. Env. Sc. 94 (2020) 100–110.
[54] C. Foti, O. Giuffrè, Interaction of ampicillin and amoxicillin with Mn^{2+}: a speciation study in aqueous solution, Molecules. 25 (2020) 3110.
[55] F. Crea, C. De Stefano, C. Foti, D. Milea, S. Sammartano, Chelating agents for the sequestration of mercury(II) and monomethyl mercury(II), Curr. Med. Chem. 21 (2014) 3819–3836.
[56] P.A.D.C. Braga, M.N. Eberlin, F.G.R. Reyes, Applicability of MALDI-TOF MS for determination of quinolone residues in fish, J. Mass Spectrom. 54 (2019) 1008–1012.
[57] M. Karas, R. Krüger, Ion formation in MALDI: the cluster ionization mechanism, Chem. Rev. 103 (2003) 427–440.
[58] E. Lehmann, R. Knochenmuss, R. Zenobi, Ionization mechanisms in matrix-assisted laser desorption/ionization mass spectrometry: contribution of pre-formed ions, Rapid Commun. Mass Spectrom. 11 (1997) 1483–1492.
[59] M. Cvijovic, V. Di Marco, P. Traldi, M.J. Stankov, P. Djurdjevic, Mass Spectrometic study of speciation in aluminium—fluoroquinolone solutions, Eur J Mass Spectrom (Chichester). 18 (2012) 313–322.
[60] R. Krüger, M. Karas, Formation and fate of ion pairs during MALDI analysis: anion adduct generation as an indicative tool to determine ionization processes, J. Am. Soc. Mass Spectrom. 13 (2002) 1218–1226.
[61] M. Juribašić, L. Bellotto, P. Traldi, L. Tušek-Božić, Electrospray ionization mass spectrometry of palladium(II) quinolinylaminophosphonate complexes, J. Am. Soc. Mass Spectrom. 22 (2011).
[62] M. Karas, M. Gluckmann, J. Schafer, Ionization in matrix-assisted laser desorption/ionization: singly charged molecular ions are the lucky survivors, J. Mass Spectrom. 35 (2000) 1–12.
[63] A.J.G. Bailey, A. Cole, J. Goodfield, P.M. May, M.E. Dreyfuss, J.M. Midgley, D. R. Williams, The complexation of transition series metal ions by nalidixic acid and related methoxyquinolones: its influence on partition coefficients with reference to antibacterial activity, Inorg. Chim. Acta 22 (1984) 283–290.

[64] A. Cole, J. Goodfield, D.R. Williams, J.M. Midgley, The complexation of transition series metal ions by nalidixic acid, Inorg. Chim. Acta 92 (1984) 91–97.
[65] Z.X. Huang, H.S. Al-Falahi, A. Cole, J.R. Duffield, C. Furnival, D.C. Jones, P. M. May, G.L. Smith, D.R. Williams, Potentiometric investigation of sparingly soluble metal-ligand systems using metal-ion buffers, Polyhedron. 1 (1982) 153–155.
[66] P.M. May, K. Murray, Database of chemical reactions designed to achieve thermodynamic consistency automatically, J. Chem. Eng. Data 46 (2001) 1035–1040.
[67] L.D. Pettit, K.J. Powell, *IUPAC Stability Constants Database*, IUPAC Editor, 2001.